Ground Penetrating Radar: Analysis of point diffractors for modeling and inversion

Albane Saintenoy, A. Tarantola

GROUND PENETRATING RADAR: ANALYSIS OF POINT DIFFRACTORS FOR MODELING AND INVERSION

ALBANE SAINTENOY AND ALBERT TARANTOLA

ABSTRACT. The three electromagnetic properties appearing in Maxwell's equations are dielectric permittivity, electrical conductivity and magnetic permeability. The study of point diffractors in a homogeneous, isotropic, linear medium suggests the use of logarithms to describe the variations of electromagnetic properties in the earth. A small anomaly in electrical properties (permittivity and conductivity) responds to an incident electromagnetic field as an electric dipole, whereas a small anomaly in the magnetic property responds as a magnetic dipole. Neither property variation can be neglected without justification. Considering radiation patterns of the different diffracting points, diagnostic interpretation of electric and magnetic variations is theoretically feasible but is not an easy task using Ground Penetrating Radar. However, using an effective electromagnetic impedance and an effective electromagnetic velocity to describe a medium, the radiation patterns of a small anomaly behave completely differently with source-receiver offset. Zero-offset reflection data give a direct image of impedance variations while large-offset reflection data contain information on velocity variations.

1. INTRODUCTION

Ground Penetrating Radar (GPR) data yield information on the electric and magnetic properties of a medium with good resolution (from a few centimeters for a 900 MHz antenna to a few meters for a 50 MHz antenna). A key issue is finding a good parameterization of the subsurface for the inverse problem, including earth media containing high magnetic permeability perturbations (ferrous metallic objects, magnetite, iron-bearing rocks,...).

It is now well understood (Tarantola, 1986; Dębski and Tarantola, 1995) that, when using multi-offset seismic data, from an elastic medium one can resolve, in order of importance, contrasts in acoustic impedance (from the reflection amplitude at small offsets), contrasts in Poisson's ratio (from the variation of reflection amplitude as a function of offset), and contrasts in mass density (being poorly resolved). These elastic parameters are nonlinear combinations of the Lamé parameters that appear explicitly in the elastic wave equation. When we started the present research, it was not obvious which functions of the three electromagnetic parameters (dielectric permittivity, electrical conductivity, and magnetic permeability) could be resolved using GPR data. Following a seismic approach (Tarantola, 1986), we show that the effective electromagnetic impedance and the effective electromagnetic velocity can be resolved.

Modeling of GPR data requires solving Maxwell's equations. One approach is to linearize Maxwell's equations by approximating the medium as a superposition of point diffractors superimposed on a smooth surrounding medium. Here we study the behavior of a single point diffractor in an isotropic, linear, homogeneous medium, excited by a propagating electromagnetic wave. The response of such a point diffractor can be found using the Stokes and Mueller matrix considering only the electrical properties (Ulaby and Elachi, 1990). We do not limit our study to the electrical properties only, we also include the magnetic properties and a magnetic point diffractor.

In addition to being relevant for inversion and modeling, a point diffractor analysis can be useful when trying to characterize an antenna radiation pattern (Arcone, 1995; Rossiter et al., 1988). The experiment consists of recording monostatic radar data over a small object in a lake or in the ground. Wrongly assuming an isotropic response from small objects adds to the uncertainty in the radiation pattern interpretation of those data. In the following we derive a first order analytical expression for the field diffracted by point diffractors, assuming small logarithmic parameter perturbations.

2. Point diffractors

2.1. **Logarithmic parameters.** GPR sends an electromagnetic wave into the ground and measures the amplitude of the back-scattered electric field. This wave consists of a coupled pair of electric field $\mathbf{E}$ and magnetic field $\mathbf{B}$. An external source, $\mathbf{J}_s$ (e.g. the current density created by a bow-tie antenna), is present in three-dimensional space R^3. To specify position, we use the coordinates x_1, x_2, x_3 with respect to an orthogonal, Cartesian reference frame with origin O and three mutually perpendicular base vectors of unit length forming a right-handed system (Figure 1). When appropriate, the space coordinates are collectively denoted by the position vector $\mathbf{x}$. The time coordinate is denoted by t.

In response to $\mathbf{J}_s$, currents result from polarization caused by displacement and conduction (Ohm's law) inside the explored medium. Electromagnetic fields in an isotropic (so parameters are scalar), linear medium with time-independent parameters, are governed by Maxwell's equations (Jackson, 1998), which in the MKSA system are,

$$\nabla \cdot (\varepsilon(\mathbf{x})\mathbf{E}(\mathbf{x},t)) \;=\; \rho(\mathbf{x},t), \tag{1}$$

$$\nabla \times \left(\frac{\mathbf{B}(\mathbf{x},t)}{\mu(\mathbf{x})}\right) \;-\varepsilon(\mathbf{x})\frac{\partial}{\partial t}\mathbf{E}(\mathbf{x},t) \;-\; \sigma(\mathbf{x})\mathbf{E}(\mathbf{x},t) \;=\; \mathbf{J}_s(\mathbf{x},t), \tag{2}$$

$$\nabla \cdot \left(\frac{\mathbf{B}(\mathbf{x},t)}{\mu(\mathbf{x})}\right) \;=\; 0, \tag{3}$$

$$\nabla \times \mathbf{E}(\mathbf{x},t) \;+\; \frac{\partial}{\partial t}\mathbf{B}(\mathbf{x},t) \;=\; \mathbf{0}, \tag{4}$$

where ρ is the density of electric charges, ∇ is the partial differential operator $[\nabla^T = (\frac{\partial}{\partial x_1}, \frac{\partial}{\partial x_2}, \frac{\partial}{\partial x_3})]$, and $\times$ indicates the cross product. The parameters appearing in these equations are dielectric permittivity ε, electrical conductivity σ, and magnetic permeability μ, which are all positive. For earth materials (Olhoeft, 1979; Olhoeft and Capron, 1993; Schön, 1996),

$$\left\{\begin{array}{rll} \varepsilon_0 & \leq \varepsilon & \leq 100\ \varepsilon_0, \\ 10^{-7}\,\mathrm{S/m} & \leq \sigma & \leq 10^{7}\,\mathrm{S/m}, \\ (1\ -\ 10^{-4})\,\mu_0 & \leq \mu & \leq 100\,\mu_0. \end{array}\right. \tag{5}$$

The reason that the dielectric permittivity ε is always greater than ε_0 (the dielectric permittivity of vacuum), is explained by Landau and Lifshitz (1960) from thermodynamic considerations. Rocks presenting exclusively diamagnetic properties are characterized by a magnetic permeability lower than μ_0 (the magnetic permeability in vacuum). For paramagnetic, ferro and ferri-magnetic rocks, $\mu > \mu_0$.

Parameters in inequalities (5) are positive and non-zero parameters. This allows the definition of logarithmic parameters ε^*, σ^* and μ^* (logarithm of the linear parameter over an arbitrarily chosen reference value) as follows,

$$\varepsilon^* = \ln\left(\frac{\varepsilon}{\varepsilon_0}\right), \tag{6}$$

$$\sigma^* = \ln\left(\frac{\sigma}{\sigma_0}\right), \tag{7}$$

and

$$\mu^* = \ln\left(\frac{\mu}{\mu_0}\right), \tag{8}$$

where $\mu_0 = 4\pi\ 10^{-7}\,\mathrm{H/m}$, $\varepsilon_0 \approx 8.854\ 10^{-12}\,\mathrm{F/m}$, and σ_0 is chosen to be 1 S/m. In the following, point diffractors will be contrasts in these time-independent logarithmic parameters and we will assess their implication upon the acquisition geometry of GPR data.

2.2. **Diffracted field using (ε, σ, μ) parameterization.** Equation (2) defines, in part, the behavior of the incident electromagnetic field created by $\mathbf{J}_s$ propagated in a homogeneous, linear and isotropic medium characterized by time-independent electromagnetic parameters ε, μ and σ. With the presence of a small anomaly, the perturbed medium parameters become $\varepsilon + \delta\varepsilon$, $\sigma + \delta\sigma$, and $\mu + \delta\mu$. The total field propagated in the perturbed medium is the sum of the incident field and the field scattered by the anomaly, $\mathbf{E} + \delta\mathbf{E}$ and $\mathbf{B} + \delta\mathbf{B}$.

We calculate the Fréchet, or functional, derivatives of the wavefield $\delta\mathbf{E}$ with respect to the medium parameters. We compute them by taking the first order of a series expansion. For example, the derivative of $\sin(x)$ is computed by expanding $\sin(x + \delta x) = \sin(x) + \cos(x)\delta x + ...$ and keeping only the first order term [i. e., the derivative of $\sin(x)$ is $\cos(x)$].

An anomaly in linear parameters, δm, is related to an anomaly in logarithmic parameters δm^* by

$$\delta m^* = (m + \delta m)^* - m^* = \ln\frac{m + \delta m}{m_0} - \ln\frac{m}{m_0} = \ln\frac{m + \delta m}{m}, \tag{9}$$

where m is either ε, σ, or μ. It follows that

$$m + \delta m = m\exp\delta m^* \approx m(1 + \delta m^*). \tag{10}$$

The interpretation of this first order approximation is examined below.

After canceling the background terms and keeping only first order terms, the perturbed parameters (10) in equation (2) yield

$$\begin{aligned}\nabla\times\left(\frac{\delta\mathbf{B}(\mathbf{x},t)}{\mu}\right) - \varepsilon\,\frac{\partial}{\partial t}\delta\mathbf{E}(\mathbf{x},t) - \sigma\,\delta\mathbf{E}(\mathbf{x},t) = \\ \nabla\times\left(\frac{\delta\mu^*(\mathbf{x})}{\mu}\,\mathbf{B}(\mathbf{x},t)\right) + \varepsilon\,\delta\varepsilon^*(\mathbf{x})\,\frac{\partial}{\partial t}\mathbf{E}(\mathbf{x},t) + \sigma\,\delta\sigma^*(\mathbf{x})\,\mathbf{E}(\mathbf{x},t).\end{aligned} \tag{11}$$

It is as if the perturbed fields, $\delta\mathbf{E}$ and $\delta\mathbf{B}$, propagate in the non perturbed medium described by parameters ε, σ and μ, and originate from virtual electric sources that are the terms on the right side in equation (11). Those secondary sources depend on logarithmic parameter variations and on the electromagnetic fields $\mathbf{E}$ and $\mathbf{B}$ that would have existed if there were no perturbations. The anomaly behaves like a secondary electric source that scatters $\delta\mathbf{E}$ and $\delta\mathbf{B}$.

When the perturbation in parameters is localized over a volume, V, centered at point $\mathbf{x}_0$, the logarithmic contrasts can be written as

$$\delta\varepsilon^*(\mathbf{x}) = A^*_\varepsilon\,\delta_{1/V}(\mathbf{x} - \mathbf{x}_0), \tag{12}$$

$$\delta\sigma^*(\mathbf{x}) = A^*_\sigma\,\delta_{1/V}(\mathbf{x} - \mathbf{x}_0), \tag{13}$$

and

$$\delta\mu^*(\mathbf{x}) = A^*_\mu\,\delta_{1/V}(\mathbf{x} - \mathbf{x}_0), \tag{14}$$

where $\delta_{1/V}(\mathbf{x}-\mathbf{x}_0)$ is a smooth function that converges to the Dirac distribution $\delta(\mathbf{x}-\mathbf{x}_0)$ as $V \to 0$. The term A^*_ε is a perturbation in the logarithmic permittivity multiplied by the perturbation volume V. It is the same with A^*_σ and A^*_μ for the logarithmic conductivity perturbation and the logarithmic permeability perturbation, respectively.

The question now becomes, what are the characteristics of the electric field diffracted by such a point source? When $\mathbf{J}_s(\mathbf{x},t) = \mathbf{J}(t)\delta(\mathbf{x} - \mathbf{x}_0)$, and $\mathbf{J}(t)$ is a density of currents independent of spatial position, there is creation of an electric field that is given by solving

$$\nabla\nabla\cdot\mathbf{E}(\mathbf{x},t) - \nabla^2\mathbf{E}(\mathbf{x},t) - \mu\varepsilon\frac{\partial^2}{\partial t^2}\mathbf{E}(\mathbf{x},t) + \mu\sigma\frac{\partial}{\partial t}\mathbf{E}(\mathbf{x},t) = -\mu\frac{\partial}{\partial t}\mathbf{J}_s(\mathbf{x},t). \tag{15}$$

This equation is the curl of equation (4) combined with the derivative of equation (2) with respect to time. The solution to equation (15) is a Green's tensor whose (p,q) component in the frequency domain is

$$G^{pq}(\mathbf{x},\omega,\mathbf{x}_0) = \frac{\exp(\mathrm{i}\omega\mathrm{r}/\mathrm{c})}{4\pi r}(\delta^{pq} - \gamma^p\gamma^q) + \frac{\mathrm{ic}}{\omega}\frac{\exp(\mathrm{i}\omega\mathrm{r}/\mathrm{c})}{4\pi r^2}(1 + \frac{\mathrm{ic}}{\omega r})(\delta^{pq} - 3\gamma^p\gamma^q), \tag{16}$$

where $p \in \{1,2,3\}$ and is the resulting electric field direction index, $q \in \{1,2,3\}$ and is the source direction index, $\mathrm{i} = \sqrt{-1}$, ω is the frequency, $r = ||\mathbf{x} - \mathbf{x}_0||$ is the distance between the observation point $\mathbf{x}$ and the source position $\mathbf{x}_0$, $c = \sqrt{1/\mu(\varepsilon + \mathrm{i}\sigma/\omega)}$ is the electromagnetic wave speed, and $\gamma^p = (x^p - x_0^p)/r$. Details on the development of this expression can be found in (Saintenoy, 1998).

When the medium has low conductivity ($\sigma \ll \varepsilon\omega$), and the second term in equation (16) is small compared to the first one ($r \gg \lambda$ where λ is the wavelength), the far-field term of the (p,q) component of the Green's tensor is written in the space-time domain as

$$G^{pq}(\mathbf{x}, t, \mathbf{x}_0, t_0) = \frac{1}{4\pi r}(\delta^{pq} - \gamma^p\gamma^q)\delta(t - t_0 - \frac{r}{c}). \tag{17}$$

The p-th component of the far-field term of the electric field diffracted when $\mathbf{J}_s(\mathbf{x}, t)$ is more general and localized at $\mathbf{x}_0$, is the time convolution of the Green's tensor with $\mathbf{J}_s$, integrated over the scattered volume,

$$\delta E^p(\mathbf{x}, t) = \int G^{pq}(\mathbf{x}, t, \mathbf{x}_0, t_0) * \mu\frac{\partial}{\partial t} J_s^q(\mathbf{x}_0, t_0) dV(\mathbf{x}_0), \tag{18}$$

with an implicit summation on the repeated indices and time convolution represented by an asterisk. Therefore, the field $\delta\mathbf{E}$ diffracted by a small perturbation in electromagnetic parameters is calculated (Saintenoy, 1998) from equation (18), using the secondary source terms expressed from equations (11), (12), (13) and (14), as

$$\begin{aligned}\delta\mathbf{E}(\mathbf{x}, t) = \frac{1}{4\pi r c^2}\Bigg[& A_\varepsilon^* \left(\mathbf{r} \times \frac{\partial^2}{\partial t^2}\mathbf{E}\left(\mathbf{x}_0, t - \frac{r}{c}\right)\right) \times \mathbf{r} \\ & + \mu\sigma c^2 A_\sigma^* \left(\mathbf{r} \times \frac{\partial}{\partial t}\mathbf{E}\left(\mathbf{x}_0, t - \frac{r}{c}\right)\right) \times \mathbf{r} \\ & + A_\mu^* \left(\mathbf{R}_{inc} \times \frac{\partial^2}{\partial t^2}\mathbf{E}\left(\mathbf{x}_0, t - \frac{r}{c}\right)\right) \times \mathbf{r}\Bigg],\end{aligned} \tag{19}$$

where $\mathbf{r}$ is the unit vector pointing from the diffracting point, $\mathbf{x}_0$, towards the observation point, $\mathbf{x}$. $\mathbf{R}_{inc}$ is the unit vector in the direction of the incident wavefront displacement (Figure 1). The diffracted magnetic field associated with the diffracted electric field is given by equation (4).

The analytical expression (19) of the diffracted electric field allows for the separation of the contribution to the total diffracted field of each type of anomaly. A point anomaly diffracts an electric field $\delta\mathbf{E}$ that is the sum of three terms. In each term of equation (19), the amplitude of $\delta\mathbf{E}$ is proportional to the volumetric contrasts A_ε^*, A_σ^* or A_μ^*, with a spatial dependence (the cross products between $\mathbf{r}$, $\mathbf{R}_{inc}$, and the incident electric field $\mathbf{E}$) and a time dependence (a first or second time derivative of the incident electric field $\mathbf{E}$). The contribution to $\mathbf{E}$ produced by A_ε^* has the same spatial dependence as the contribution produced by A_σ^*, but does not have the same time dependence. The distribution of the diffracted field amplitude, normalized to its maximum value, over a sphere centered at the point anomaly is called a radiation pattern. Thus, to have the same spatial dependence implies the same radiation pattern. Taken separately, an anomaly in dielectric permittivity has the same spatial radiation pattern as an anomaly in electrical conductivity, but does not have the same spatial radiation pattern as an anomaly in magnetic permeability. Therefore, considering only two types of point diffractors, an electric point diffractor and a magnetic point diffractor, is justified if we are interested only in the spatial radiation pattern and not in the time dependence of the signal.

It should be noted that the contribution to the total field of the contrast in electrical conductivity is proportional to the electrical conductivity of the surrounding medium, σ. In our case where we consider only low-conductive media, this contribution will be small.

2.3. **Radiation and polarization patterns.** Expression (19) shows that each type of diffracting point can be described by a radiation pattern and a polarization pattern (display of the diffracted electric field polarization and amplitude over a sphere centered at the point anomaly). The

radiation pattern for an electric diffracting point (Figure 2a) is a torus centered at the point anomaly. No electric field is diffracted in the direction of electric incident field (the axis of the torus). The corresponding polarization pattern (Figure 2b) shows that the diffracted electric field is poloidal, whereas the diffracted magnetic field is toroidal. These patterns are the same as those obtained in the far-field for a small electric dipole subjected to an incident electromagnetic field, where the axis of the electric dipole is parallel to the incident electric field.

A magnetic diffracting point behaves, in the far-field, like a small magnetic dipole when it is subjected to an electromagnetic field. The diffracted magnetic field is the same that of the electric field diffracted by a small electric dipole parallel to the incident magnetic field. Figure 3a displays the magnetic dipole radiation pattern, which is a torus perpendicular to that in Figure 2a. Figure 3b shows the corresponding polarization pattern. The magnetic field diffracted by a magnetic diffracting point is poloidal, whereas the diffracted electric field is toroidal.

2.4. **Point diffractor in (ε_e, μ) and (Z, c) parameterizations.** A point contrast in electrical conductivity diffracts an electromagnetic field with the same radiation pattern as that of a point contrast in dielectric permittivity. However the field diffracted by the conductivity contrast alone depends on the first-time derivative of the incident electric field, whereas, the field diffracted by the permittivity contrast alone depends on the second-time derivative of the electric incident field [equation (19)]. Therefore, dielectric permittivity and conductivity can be merged, introducing a fictitious time dependence of the electric parameter, into the effective dielectric permittivity ε_e,

$$\varepsilon_e \delta(t) = \varepsilon \delta(t) + \sigma \mathrm{H}(t), \tag{20}$$

where $\mathrm{H}(t)$ is the Heaviside function. In the Fourier domain, considering an harmonic dependent electromagnetic field, the effective dielectric permittivity is

$$\varepsilon_e \;=\; \varepsilon + \frac{\sigma}{\mathrm{i}\omega}, \tag{21}$$

where ω is the incident field frequency (Jackson, 1998). With factorization of this parameter, equation (2) becomes

$$\nabla \times \left(\frac{\mathbf{B}(\mathbf{x},t)}{\mu(\mathbf{x})} \right) \;-\; \varepsilon_e(\mathbf{x}) * \frac{\partial}{\partial t} \mathbf{E}(\mathbf{x},t) \;=\; \mathbf{J}_s(\mathbf{x},t). \tag{22}$$

Following the above approach, a small perturbation in logarithmic effective permittivity, subjected to an incident electromagnetic field, acts as a secondary source of current density,

$$\mathbf{J}_s(\mathbf{x},t) \;=\; \varepsilon_e(\mathbf{x}) \delta \varepsilon_e^*(\mathbf{x}) * \frac{\partial}{\partial t} \mathbf{E}(\mathbf{x},t). \tag{23}$$

Consequently, a point anomaly that is described by

$$\delta \varepsilon_e^*(\mathbf{x}) \;=\; A_{eff}^* \; \delta_{1/V}(\mathbf{x} - \mathbf{x}_0), \tag{24}$$

and

$$\delta \mu^*(\mathbf{x}) \;=\; A_{\mu}^* \; \delta_{1/V}(\mathbf{x} - \mathbf{x}_0), \tag{25}$$

in an isotropic, homogeneous, linear, low-conductivity medium diffracts an electric field (Saintenoy, 1998)

$$\begin{aligned} \delta \mathbf{E}(\mathbf{x},t) \;=\; \frac{\varepsilon \mu}{4\pi r} \Bigg[& A_{eff}^* * \left(\mathbf{r} \times \frac{\partial^2}{\partial t^2} \mathbf{E}\left(\mathbf{x}_0, t - \frac{r}{c} \right) \right) \times \mathbf{r} \\ & + A_{\mu}^* * \left(\mathbf{R}_{inc} \times \frac{\partial^2}{\partial t^2} \mathbf{E}\left(\mathbf{x}_0, t - \frac{r}{c} \right) \right) \times \mathbf{r} \Bigg]. \end{aligned} \tag{26}$$

Terms A_{eff}^* and A_{μ}^* are the perturbations in logarithmic parameters ε_{eff}^* and μ^* multiplied by the volume of the anomaly.

Another parameterization must be considered as well. The effective impedance Z and the effective velocity c defined from the magnetic permeability and the effective dielectric permittivity as

$$Z = \sqrt{\frac{\mu}{\varepsilon_e}} \tag{27}$$

and

$$c = \sqrt{\frac{1}{\mu\varepsilon_e}}. \tag{28}$$

Then, combining (24) and (25) with (27) and (28) results in

$$A_Z^* \;=\; \frac{1}{2}(A_\mu^* - A_{eff}^*) \tag{29}$$

and

$$A_c^* \;=\; \frac{1}{2}(-A_\mu^* - A_{eff}^*). \tag{30}$$

Terms A_Z^* and A_c^* are the perturbations in logarithmic parameters Z^* and c^* multiplied by the volume of the anomaly. Using A_Z^* and A_c^*, equation (26) becomes (Saintenoy, 1998)

$$\begin{aligned}\delta\mathbf{E}(\mathbf{x},t) \;=\; \frac{\varepsilon\mu}{4\pi r}\Bigg[A_Z^* * \left((-\mathbf{r}+\mathbf{R}_{inc})\times\frac{\partial^2}{\partial t^2}\mathbf{E}\left(\mathbf{x}_0, t-\frac{r}{c}\right)\right)\times\mathbf{r} \\ - A_c^* * \left((\mathbf{r}+\mathbf{R}_{inc})\times\frac{\partial^2}{\partial t^2}\mathbf{E}\left(\mathbf{x}_0, t-\frac{r}{c}\right)\right)\times\mathbf{r}\Bigg].\end{aligned} \tag{31}$$

The radiation and polarization patterns defined by equation (31), associated with a point diffractor described by the parameters Z and c, are displayed in Figures 4 and 5.

3. DISCUSSION

3.1. **Validity of the diffracted field analytical expressions.** The derivation of expressions (19), (26) and (31), required many assumptions in addition to isotropy and linearity. First, to simplify the expression of the Green's tensor and to use it in the time domain, only the far-field term was considered,

$$\lambda \;\ll\; r, \tag{32}$$

and, the conductivity of the surrounding medium was assumed to be small,

$$\sigma \;\ll\; \varepsilon\omega. \tag{33}$$

To model some actual GPR data, the computation should be done in the frequency domain and the complete expression of the Green's tensor (16) should be used. However, to get a diagnostic characterization, of the effects of anomalies in electrical and magnetic properties in a homogeneous medium, on the diffracted electric field, assumption (33) is not limiting. Indeed, an electrical conductivity anomaly has the same radiation pattern as a dielectric permittivity anomaly. However, because of assumption (32) our diagnostic will be correct only for far-field data.

An approach for analyzing scattering effects in a dispersive medium is discussed in Saintenoy (1998). In this paper, the relative importance of electrical and magnetic effects are discussed for a single frequency. Only non-dispersive media are considered. The frequency dependence will be the subject of future work and is not discussed here.

A less obvious aspect should be noted about our computation of equation 19. We wish to perform the modeling of the wavefield using a first order approximation (it happens that "first order (Taylor) approximation" and "first order Born approximation" are equivalent). We linearize equations (10) and keep only first order terms in equation (11). To actually use an approximation like $\exp[\delta m^*(\mathbf{x})] \;=\; 1 \;+\; \delta m^*(\mathbf{x})$, $\delta m^*(\mathbf{x})$ has to be small in some sense. A sensible measurement of the smallness of a function is that the L_2-norm of the function,

$$||\delta m^*(\mathbf{x})||_2 \;=\; V|\delta m^*|, \tag{34}$$

must be small. Practically, in our context, the linearization is valid when

$$|A_m^*| \ll\; \lambda^3, \tag{35}$$

with m being ε, σ and μ successively. If the logarithmic parameter contrast goes to infinity, the perturbation volume will have to go to zero in order for the Born approximation to be true.

This criterion is consistent with several papers (de Hoop, 1991; Gritto et al., 1995; Hudson and Heritage, 1981) where the domain of validity of the Born approximation is discussed.

3.2. **Importance of each parameter in the (ε, σ, μ) set.** Expression (19) of the diffracted field allows for the comparison of the relative importance of contrasts in the three parameters ε, σ and μ. For a monochromatic incident electric field $\mathbf{E}$, the maximum amplitude of the field diffracted by a dielectric permittivity anomaly is

$$|\delta\mathbf{E}|_\varepsilon = \frac{1}{4\pi r c^2} A_\varepsilon^* \omega^2 |\mathbf{E}|, \tag{36}$$

by an electrical conductivity anomaly,

$$|\delta\mathbf{E}|_\sigma = \frac{1}{4\pi r} \mu\sigma A_\sigma^* \omega |\mathbf{E}|, \tag{37}$$

and by magnetic permeability anomaly,

$$|\delta\mathbf{E}|_\mu = \frac{1}{4\pi r c^2} A_\mu^* \omega^2 |\mathbf{E}|, \tag{38}$$

with ω as the frequency of the incident wave. The contributions of ε, σ, μ are then proportional to $\varepsilon A_\varepsilon^* \omega$, σA_σ^* and $\varepsilon A_\mu^* \omega$, respectively.

Consider a small sphere composed of a mixture of 20% iron filings and 80% silica sand matrix, in a surrounding homogeneous dry sand, subjected to an electromagnetic field of frequency 600 MHz. Assume the sphere is small enough and deep enough to satisfy assumptions (32) and (35). Realistic parameter values for the mixture of iron filings and silica sand matrix $(\varepsilon_a, \sigma_a, \mu_a)$ and the dry sand $(\varepsilon, \sigma, \mu)$ can be found in Olhoeft and Capron (1993),

$$\begin{aligned} \varepsilon &= 2.2\ \varepsilon_0, & \varepsilon_a &= 2.8\ \varepsilon_0, \\ \mu &= \mu_0, & \mu_a &= 1.2\ \mu_0, \\ \sigma &= 4.6\ 10^{-5}\ \text{S/m}, & \sigma_a &= 6.92\ 10^{-5}\ \text{S/m}. \end{aligned}$$

Since

$$\varepsilon\omega \approx 0.01 S/m, \tag{39}$$

we verify that $\sigma \ll \varepsilon\omega$. Then,

$$\varepsilon \ln \frac{\varepsilon_a}{\varepsilon} \omega \approx 2.8\, 10^{-3}\ \text{S/m}$$

for the dielectric permittivity contrast contribution,

$$\sigma \ln \frac{\sigma_a}{\sigma} \approx 1.9\, 10^{-5}\ \text{S/m}$$

for the electrical conductivity contrast contribution, and

$$\varepsilon \ln \frac{\mu_a}{\mu} \omega \approx 2.2\, 10^{-3} \text{S/m}$$

for the magnetic permeability contrast contribution.

In this example, the electric conductivity contrast contribution is negligible compared to that of the two other contributions. Terms in front of the dielectric permittivity and magnetic permeability contrasts are proportional to ω while the electrical conductivity contrast contribution does not depend on ω, and the surrounding medium has low conductivity. However, this example was chosen to highlight that the contribution of the permeability contrast to the amplitude of the total diffracted field can not be neglected *a priori*. Lázaro-Mancilla *et al.* (1996) find the same result but think that the magnetic permeability does not vary significantly in most earth materials. On the other hand, ferrous metals, magnetite, hematite have relative permeability values that differ significantly from 1. Olhoeft and Capron's report (1993) contains measurements of several natural sands with relative magnetic permeabilities higher than 1.2. Olhoeft (1998) emphasizes that the materials found on Mars have relative magnetic permeability significantly greater than 1 as do sampled soils coming from Arizona, Idaho, Colorado, Hawaii, Australia and Canada (Olhoeft, personal communication). Relative magnetic permeability higher than 1 is more common than

people would like to think. Therefore we cannot neglect the magnetic permeability effect on radar data without an explicit justification.

3.3. **New geometry of acquisition ?** From equation (19), the radiation and polarization patterns associated with contrasts in each parameter are displayed in Figures 2 and 3. Figures 6 and 7 summarize the same information on radiation and polarization, showing the effects of different acquisition geometries. For example, the electromagnetic field diffracted by a point anomaly recorded with zero-offset measurements is shown in the middle of Figures 6a and 7a. The diffracted field in both cases has the same polarization direction. Magnetic and electric effects are then indistinct in a zero-offset GPR experiment.

Acquisition using two radar antennas parallel to each other and perpendicular to the acquisition profile consists of recording the diffracted field along the X_2 axis. Along this axis, the amplitude of the diffracted field is constant with the offset in Figure 6a, whereas it is decreasing with the offset in Figure 7a. Therefore, when data are recorded with both antennas 90° to the plane of acquisition, the dielectric behavior differs from the magnetic behavior. For a magnetic anomaly, the amplitude of the diffracted field depends on the offset; this is not true for a dielectric anomaly.

When using two radar antennas parallel to each other and parallel to the acquisition profile, the field diffracted by an anomaly is recorded along the X_1 axis. Along this axis, the amplitude of the diffracted field decreases with the offset in Figure 6a, whereas it is constant with the offset in Figure 7a (because of the deformation due to the projection on a plane, it might be easier to look at the 3D radiation pattern in this case). Thus, when recording data with both antennas parallel to the plane of acquisition, the amplitude depends on the offset for a dielectric anomaly, and for a magnetic anomaly it does not.

Another interesting method for acquisition of data would be to place the source antenna at 45° from the profile direction. The result of this experiment would be seen along an axis that comes in at an angle of 45° to the X_1 and X_2 axes, in Figures 6a and 7a. The electric field diffracted by a dielectric point anomaly would not be in the same direction as that diffracted by a magnetic point anomaly. Consequently, multi-component measurements can, in this case, help to distinguish magnetic effects from dielectric effects. Unfortunately, the 3 dB beam width of a finite-size resistively loaded horizontal electric dipole lying on a low-loss dielectric half-space is roughly 50° (Arcone, 1995). Thus, our theoretical observations might be hampered in real GPR experiments by the wide radiation pattern of the antennas.

3.4. **The inversion parameters: Z and c.** Because of the difficulty in separating magnetic and dielectric effects, Z and c will be the keys to the inverse problem. Indeed, Figures 4 and 5 show that zero-offset data are governed by the variations in the electromagnetic impedance alone, whereas large-offset data contain information on the effective velocity. To illustrate this behavior, reconsider the 5 cm sphere composed of a mixture of 20% iron fillings and 80% of silica sand matrix, at 4 meter depth in a homogeneous dry sand, and imagine a Common Midpoint GPR experiment centered above the sphere with antennas centered at 600 MHz.

The source antenna is emitting an electric field $\mathbf{E}$ that behaves with respect to time as a second order Ricker function,

$$\mathbf{E}(\mathbf{x}_0, t) = -\frac{c}{4\pi k r_0}(1 - 2\pi k^2 (t - \frac{r_0}{c})^2) \exp[-\pi k^2 (t - \frac{r_0}{c})^2], \tag{40}$$

where c is the wave speed in the dry sand, k equals 600 MHz, and r_0 is the distance between the source antenna and the sphere; this distance depends on the offset between the two radar antennas. The antenna radiation pattern is that of a small dipole at an interface between air and the host medium, for which equations are given by Engheta (1982).

Realistic parameter values for the mixture of iron fillings and silica sand matrix $(\varepsilon_a, \sigma_a, \mu_a)$ and dry sand $(\varepsilon, \sigma, \mu)$ have been given in the preceding numerical example. It follows that the speed of the propagating wave in dry sand is

$$c \approx \sqrt{\frac{1}{\mu_0\, 2.2\, \varepsilon_0}} \approx 0.2 \text{ m/ns}, \tag{41}$$

its main wavelength,

$$\lambda \approx \frac{c}{k} \approx 0.33 \text{ m}, \tag{42}$$

and, the product of dry sand dielectric constant and the dominant frequency,

$$\varepsilon\omega \approx 1.1\ 10^{-2}\ \text{S}/m. \tag{43}$$

Those numerical values satisfy conditions (32), (33), and (35).

Introducing the expressions for the incident electric field (40), and for the anisotropic antenna radiation pattern in equation (19), a synthetic radargram is computed (Figure 8a), assuming that the antennas are perpendicular to the plane of acquisition. Note that other planes could have been chosen as the field is diffracted in 3 dimensions. The geometric dispersion is included in equations (40) and (19). Then the contributions of the impedance contrast and the velocity contrast are calculated (Figures 8b and 8c).

Trace to trace maximum amplitudes, normalized to the maximum amplitude of the zero-offset trace, are presented in Figure 9. Figure 9a results from the calculation using antenna radiation pattern expressions from Engheta (1982). In Figure 9b, we use omnidirectional antenna radiation patterns to show that the amplitude peaks at 3.8 m are caused by the radiation pattern of the point dipole antennas. However, in our example, A_Z^* ($\approx -1.5\,10^{-5}$ m^3) is 7 times less than A_c^* ($\approx -11.1\,10^{-5}$ m^3), so, even with the geometrical dispersion, the amplitude is, at first, increasing when the offset between the two antennas increases. To conclude this numerical application, Figure 9 emphasizes that, independent from antenna radiation patterns, the electric field recorded at zero offset depends only on the effective impedance contrast, and, the effective velocity contrast contribution dominates for half-offsets larger than 2 m in this case.

4. Conclusions

We have studied a point diffractor in a homogeneous, linear, isotropic, low-conductivity medium, using different parameterizations and have made several observations useful for GPR acquisition. First, by studying the amplitude of the field diffracted by a small anomaly, it has been shown that magnetic variations of the ground cannot be ignored without overwhelming justification.

In the far field approximation, a point logarithmic effective dielectric permittivity anomaly acts as a small electric dipole. A point logarithmic effective magnetic permeability anomaly acts as a small magnetic dipole. These behave differently. Therefore, dielectric and magnetic effects can be theoretically distinguished with GPR surface data, by varying the antenna orientations. However, it remains difficult to apply in real life because of the lack of precision in antenna directionality.

Instead of parameterizing a medium with dielectric and magnetic parameters, we may use effective electromagnetic impedance and effective electromagnetic velocity. Radiation patterns show that this parameterization is very useful for the inverse problem. Indeed, the effective impedance controls the amplitude reflected at small offsets, whereas the effective velocity controls the amplitude reflected at large offsets. It implies that a multi-offset data acquisition allows a multi-parameter measurement. A radar image obtained in monostatic mode is a direct image of the effective impedance contrasts. A radar image obtained with a large offset between the source and the receiver contains information about effective velocity contrasts.

In terms of 3D modeling, the equations developed in this paper provide a valid starting point given the limitations outlined previously. However a good model should take into account the near-field, and a conductive and dispersive medium. This can be done considering the near-field term in the expression of the Green's tensor and staying in the frequency domain. This is the subject of future work.

5. Acknowledgments

This work was supported by the Bureau de Recherche Géologique et Minière (Orléans). Comments and suggestions by John Scales, Gary Olhoeft, and the reviewers are gratefully acknowledged.

6. References

Arcone, S. A., 1995, Numerical studies of the radiation patterns of resistively loaded dipoles: J. Appl. Geophys., **33**, 39–52.

Dębski, W., and Tarantola, A., 1995, Information on elastic parameters obtained from amplitude of reflected waves: Geophysics, **60**, no. 5, 1426–1436.

de Hoop, A. T., 1991, Convergence criterion for the time-domain iterative Born approximation to scattering by an inhomogeneous, dispersive object: J. Opt. Soc. Am. A, **8**, no. 8, 1256–1260.

Engheta, N., and H., P. C., 1982, Radiation patterns of interfacial dipole antennas: Radio Science, **17**, 1557–1566.

Gritto, R., Korneev, V. A., and Johnson, L. R., 1995, Low-frequency elastic-wave scattering by an inclusion: limits of applications: Geophys. J. Int., **120**, 677–692.

Hudson, J. A., and Heritage, J. R., 1981, The use of the Born approximation in seismic scattering problems: Geophys. J. R. astr. Soc., **66**, 221–240.

Jackson, J. D., 1998, Classical electrodynamics: John Wiley & Sons, Inc.

Landeau, L., and Lifshitz, E., 1960, Electrodynamics of continuous media: Addison-Wesley, Publ. Co.

Lázaro-Mancilla, O., and no, E. G.-T., 1996, Synthetic radargrams from electrical conductivity and magnetic permeability variations: J. Appl. Geophys., **34**, 283–290.

Olhoeft, G. R., and Capron, D. E., 1993, Laboratory measurements of the radiofrequency electrical and magnetic properties of soils from near Yuma, Arizona: U. S. Geol. Surv. Open File Report 93-701.

Olhoeft, G., 1979, Tables of room temperature electrical properties for selected rocks and minerals with dielectric permittivity statistics: U. S. Geol. Surv. Open File Report 79-993.

Olhoeft, G. R., 1998, Groung penetrating radar on Mars: *in* Proc. of GPR'98, 7th Int. Conf. on Ground Penetrating Radar, Univ. of Kansas, 387–392.

Rossiter, J. R., Reimer, E. M., Lalumiere, L., and Inkster, D. R., 1988, Radar cross-section of fish at VHF: *in* Pilon, J. A., (ed.), Ground Penetrating Radar: Geol. Surv. Canada, paper 90-4,199-202.

Saintenoy, A., 1998, Radar géologique: acquisition multi-déports pour une mesure multi-paramètres: Ph.D. thesis, Univ. Paris 7.

Schön, J. H., 1996, Physical properties of rocks: fundamentals and principles of petrophysics: Pergamon Press, Inc.

Tarantola, A., 1986, A strategy for nonlinear elastic inversion of seismic reflection data: Geophysics, **51**, 1893–1903.

Ulaby, F. T., and Elachi, C., 1990, Radar polarimetry for geoscience applications: Artech house, Inc.

Institut de Physique du Globe, 4, place Jussieu, 75252 Paris Cedex 05, France, Colorado School of Mines, Department of Geophysics, Golden CO 80403, USA

Institut de Physique du Globe, 4, place Jussieu, 75252 Paris Cedex 05, France

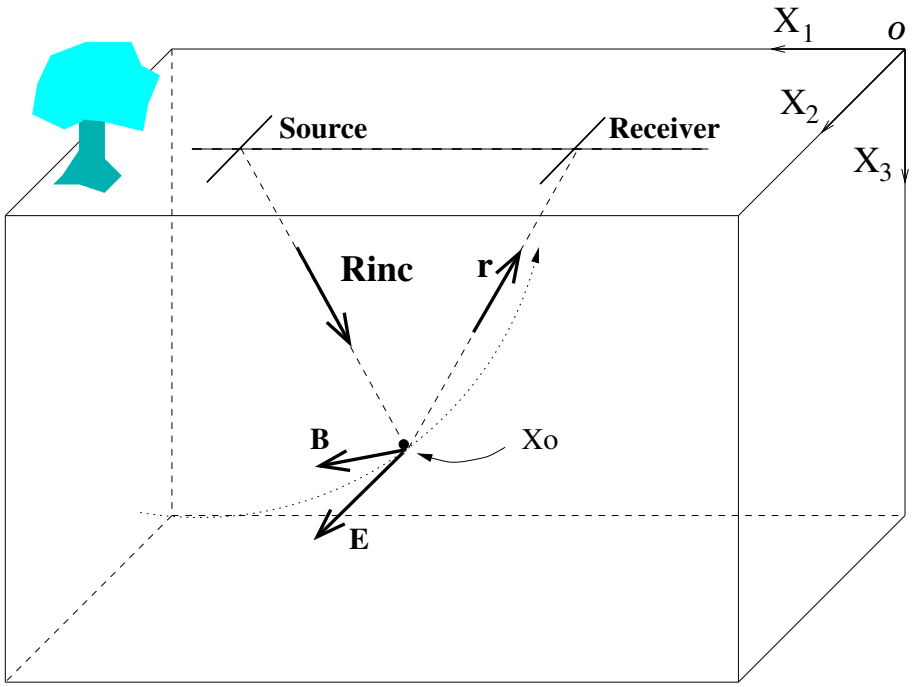

FIGURE 1. Position of the antennas and polarization of incident electromagnetic fields **E** and **B** when arriving at the anomaly at point $\mathbf{x}_0$.

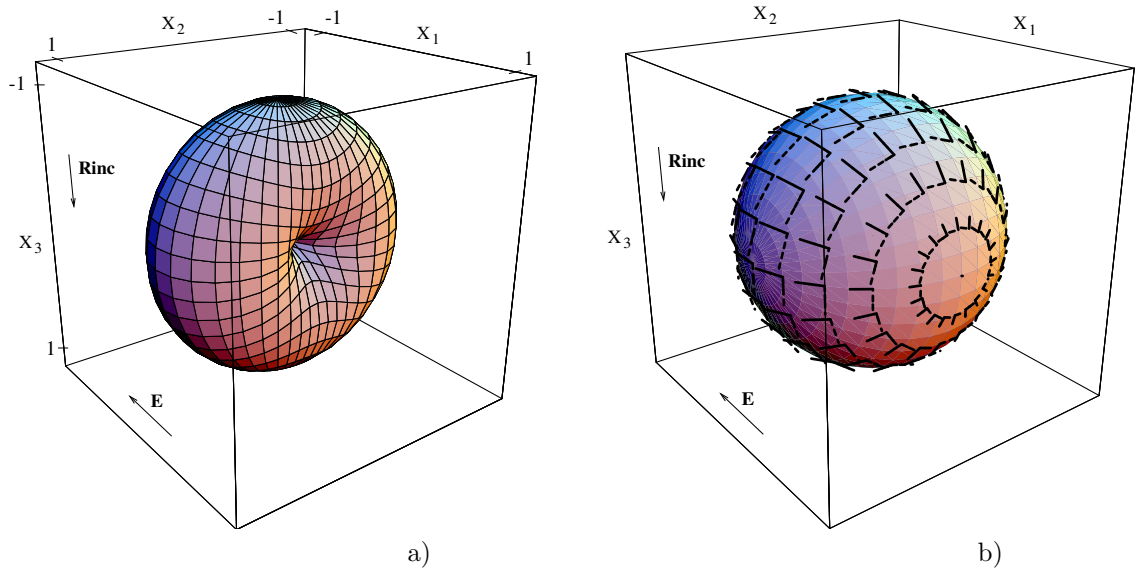

FIGURE 2. (a) Radiation and (b) polarization patterns of a positive electric point anomaly when illuminated by an electromagnetic wave moving in the $\mathbf{R}_{inc}$ direction with an electric field **E** in the X_1 direction. In (b), the diffracted electric field (solid lines) is poloidal whereas the corresponding magnetic field (dashed lines) is toroidal.

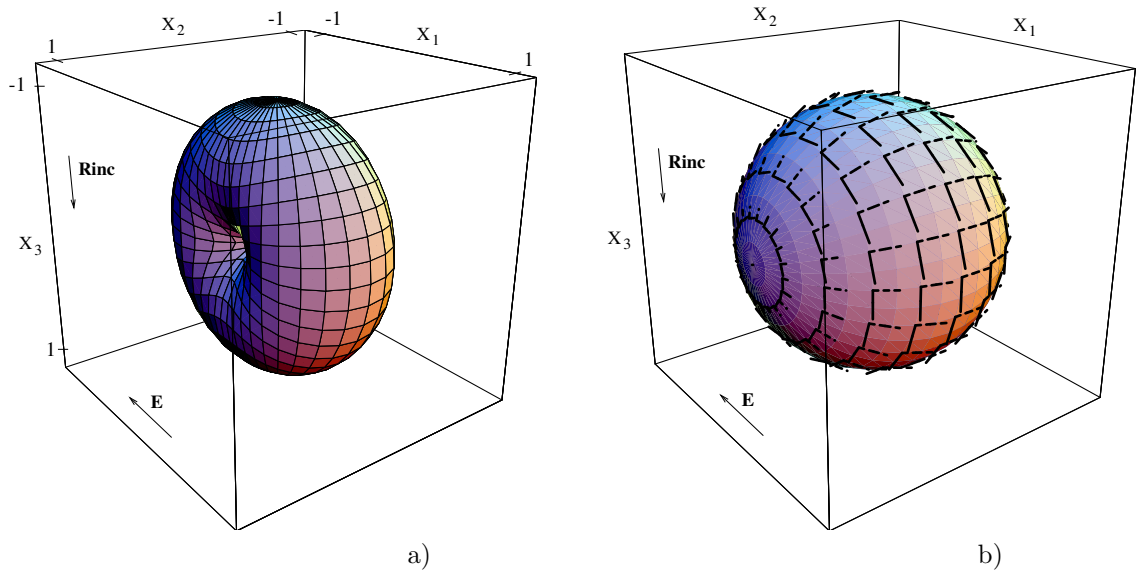

FIGURE 3. (a) Radiation and (b) polarization patterns of a positive magnetic point anomaly when illuminated by an electromagnetic wave moving in the $\mathbf{R}_{inc}$ direction with an electric field $\mathbf{E}$ in the X_1 direction. In (b), the diffracted electric field (solid lines) is toroidal whereas the corresponding magnetic field (dashed lines) is poloidal.

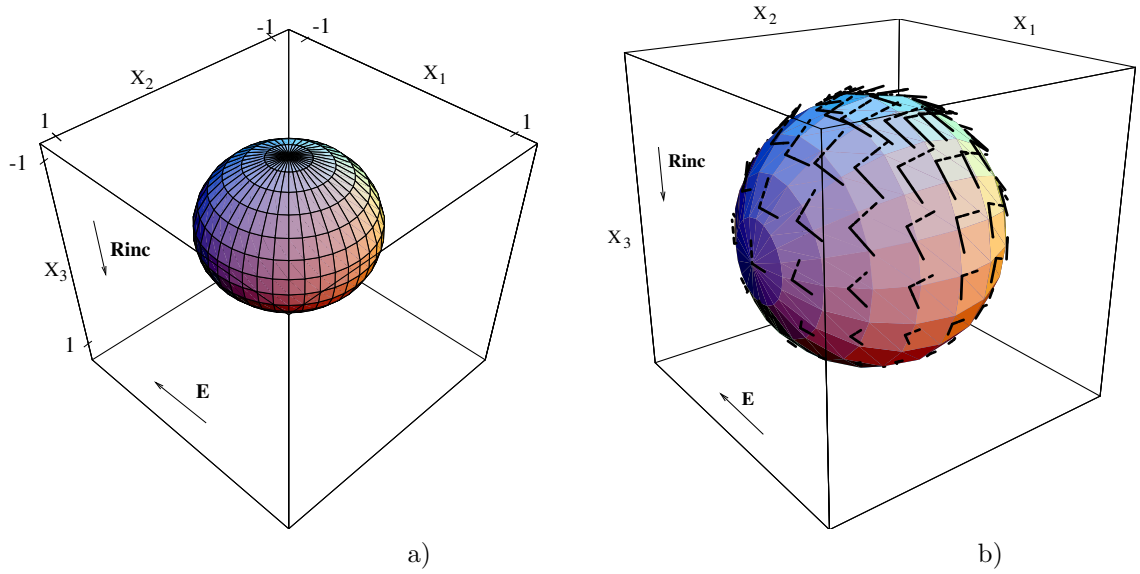

FIGURE 4. (a) Radiation and (b) polarization patterns of a positive impedance point anomaly when illuminated by an electromagnetic wave moving in the $\mathbf{R}_{inc}$ direction with an electric field $\mathbf{E}$ in the X_1 direction. In (b), the diffracted electric field is represented by solid lines, and its associated magnetic field by dashed lines, on the sphere.

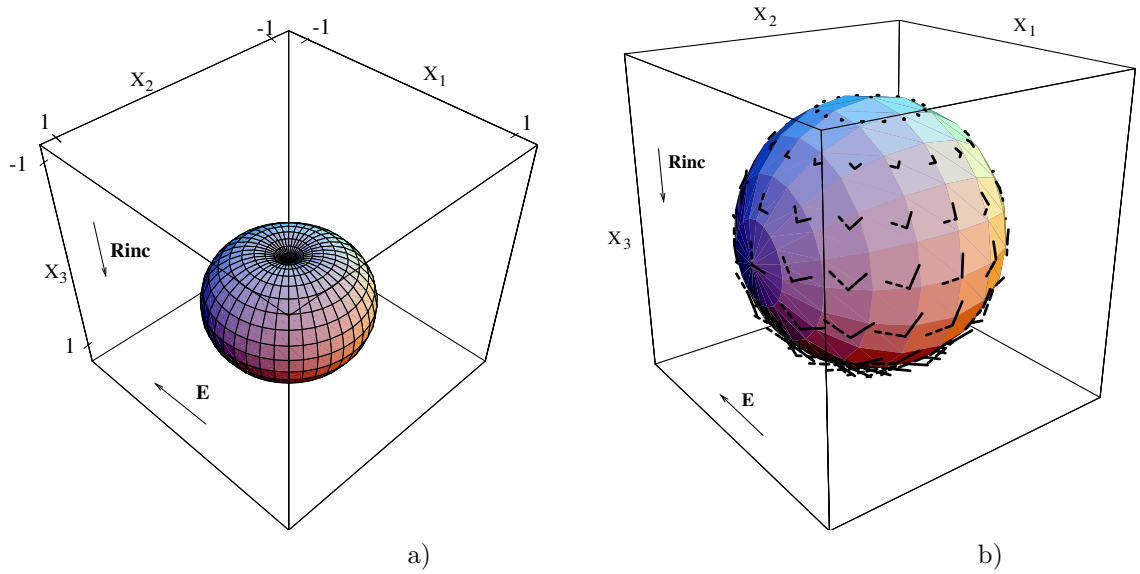

FIGURE 5. (a) Radiation and (b) polarization of a positive velocity anomaly when illuminated by an electromagnetic wave moving in the $\mathbf{R}_{inc}$ direction with an electric field $\mathbf{E}$ in the X_1 direction. In (b), the diffracted electric field is represented by solid lines, and its associated magnetic field by dashed lines, on the sphere.

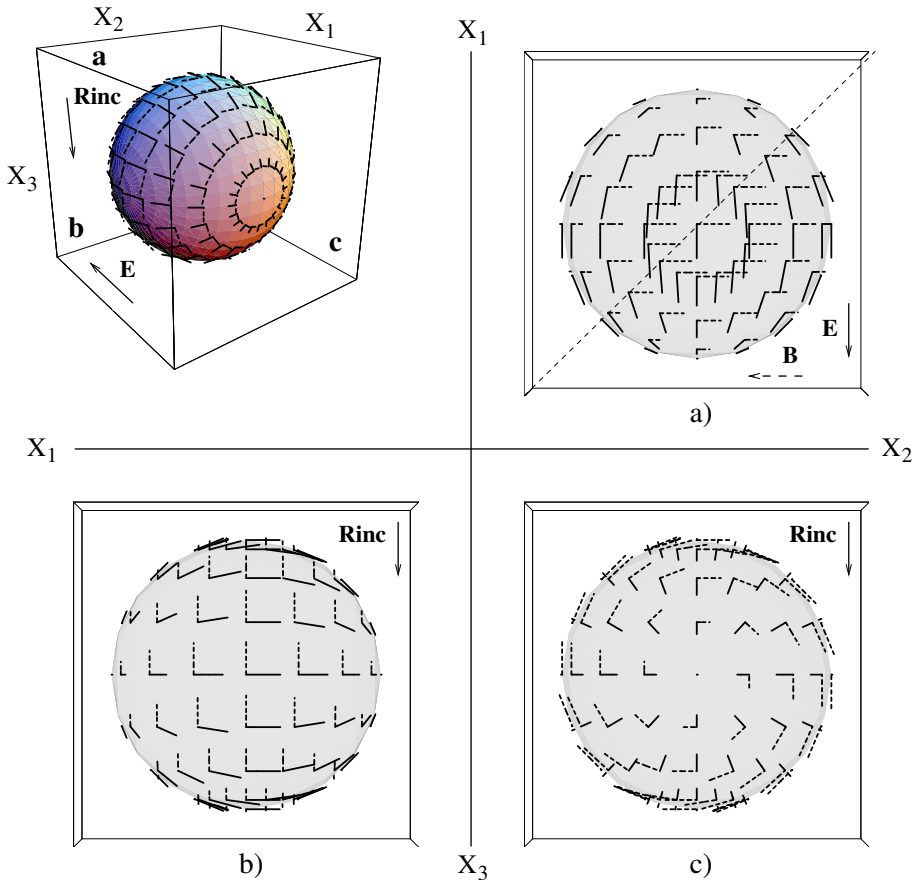

FIGURE 6. To visualize the effects of different acquisition geometries on GPR data due to an electric point diffractor, Figure 2b is redisplayed here (upper left) and viewed along the three axis; (a) along the X_3 axis; (b) along the X_2 axis; (c) along the X_1 axis.

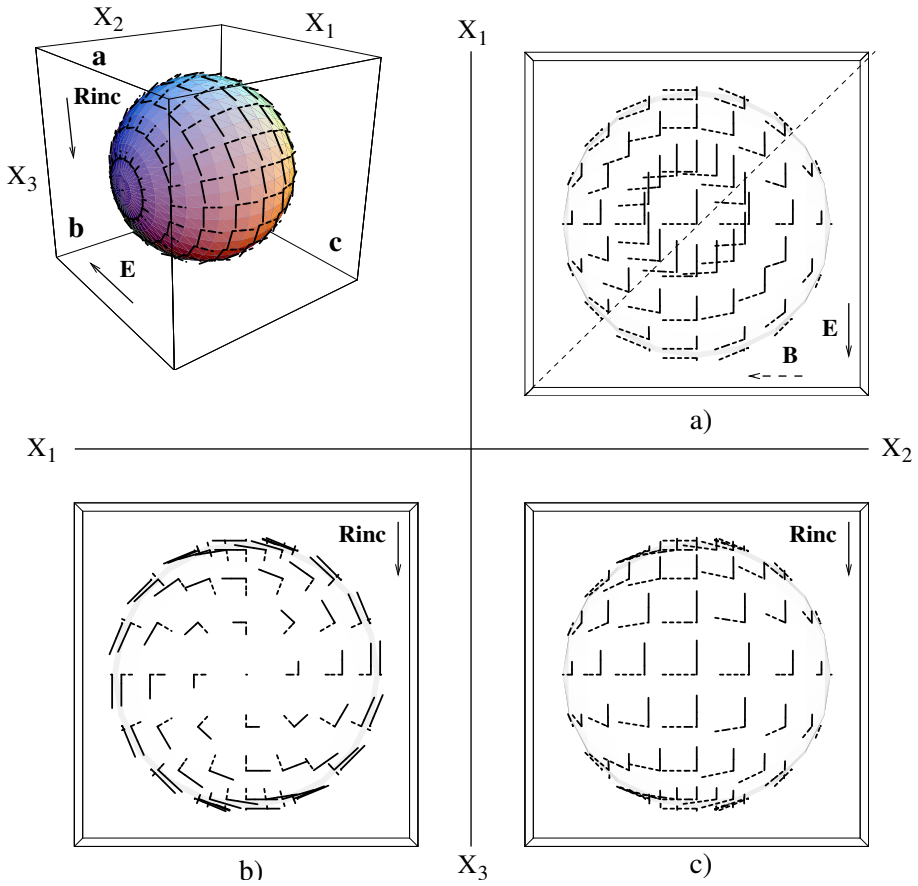

FIGURE 7. To visualize the effects of different acquisition geometries on GPR data due to a magnetic point diffractor, Figure 2b is redisplayed here (upper left) and viewed along the three axis; (a) along the X_3 axis; (b) along the X_2 axis; (c) along the X_1 axis.

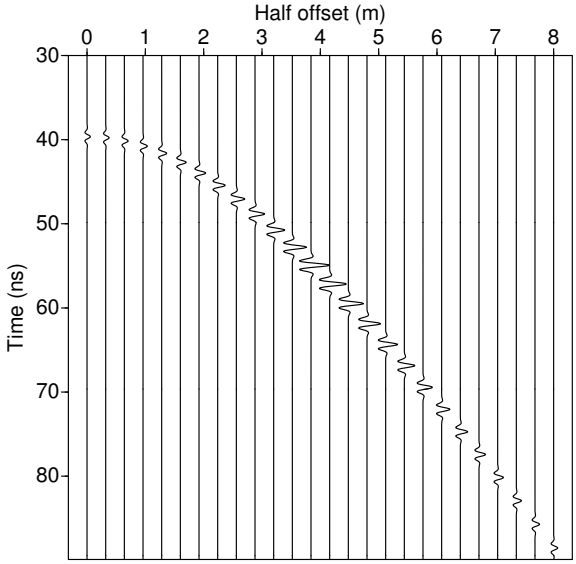
Half offset (m)
0 1 2 3 4 5 6 7 8
Time (ns)
30 40 50 60 70 80

a)

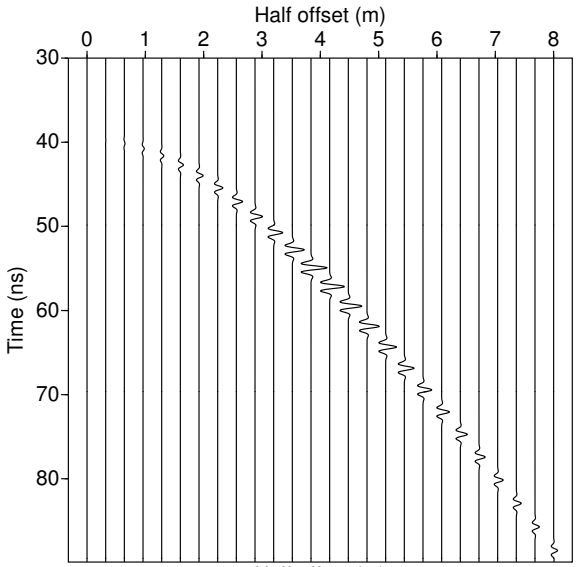
Half offset (m)
0 1 2 3 4 5 6 7 8
Time (ns)
30 40 50 60 70 80

b)

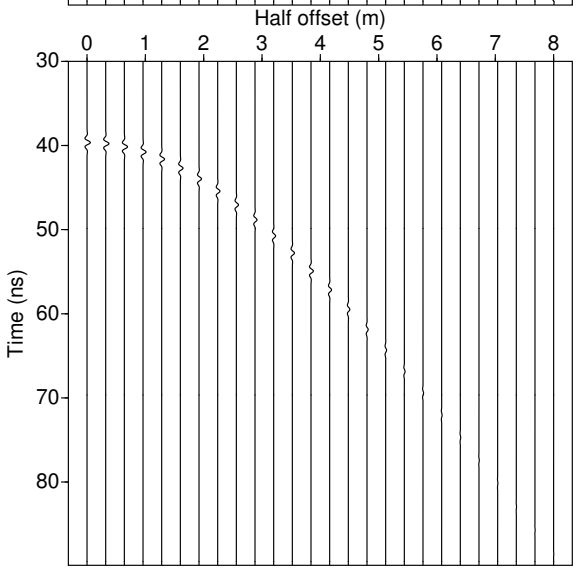
Half offset (m)
0 1 2 3 4 5 6 7 8
Time (ns)
30 40 50 60 70 80

c)

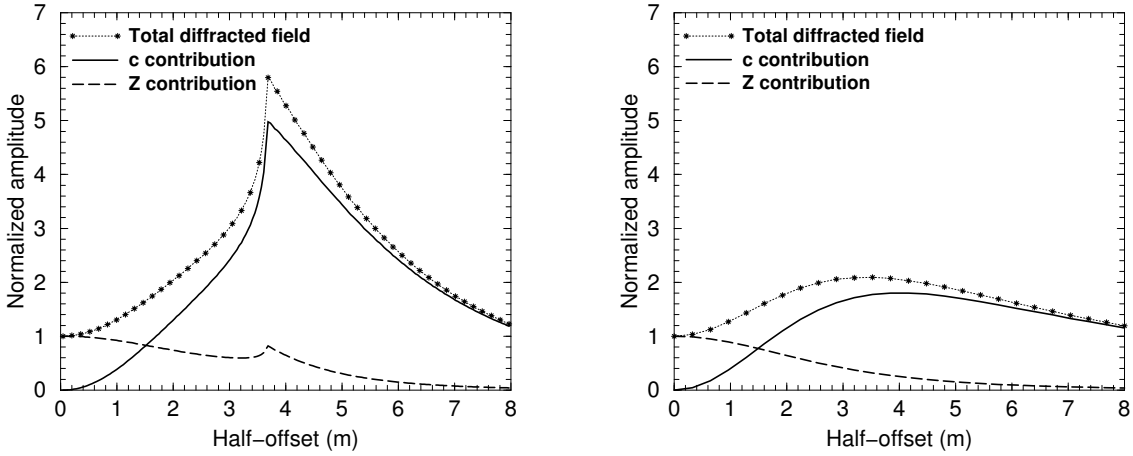

a) b)

FIGURE 9. (a) Trace to trace maximum amplitude, normalized to the maximum amplitude of the zero-offset trace, of the radargrams in Figure 8 recomputed with 4 times as many traces. For clarification, amplitudes have been recalculated and displayed in (b) for omnidirectional source and receiver. In this numerical example, A_Z^* is 7 times less than A_c^*, so, even with the geometric dispersion, the amplitude first increases with the offset. Large offset data contain mainly information on velocity contrasts.